Determining the Height of Satellites at the Zenith using Angular Velocity

Team members:

Laura Brijan
Smrithi Chandra
Samir Haffegee
Kateryna Kryvobokova
Miguel Miralda
Mathias Perazo
Emma Small
Nils Thiessen
Indra Vezbergaite

Maastricht Science Programme

Supervisor: Chad Ellington

Date: 3-7-2023

Word count: 5819

Table of Contents

Introduction

When looking at the sky, one might see bright points moving along it. A common misconception is that they might be planes or shooting stars, but often they are satellites. The first satellite successfully launched into orbit was Sputnik 1, launched by the Soviet Union in 1957 (Tatem et al., 2008). Since then, satellites have been adopted for many uses. Two types of satellites, meteorological and communication, provide the general public with diverse information and services. Generally, these types of satellites orbit the Earth at low altitudes, between 160 and 1600 kilometres above the Earth's surface (Stewart, n.d.). Consequently, Low Earth Orbit satellites (LEOs) often appear relatively bright to the spectator and tracking them in the night sky is possible. Because of this, one could potentially determine properties such as the height and angular velocity of these satellites.

Calculating distances from astronomical observations is generally done by employing one of two techniques; the parallax method and the radar method. The parallax method uses triangulation, which utilises measurements taken in two different places to measure spatial distances of stars. The radar method, making use of radar technology, is suitable for distances within the solar system (Fraknoi et al., 2022). In this paper, a third technique will be investigated. A formula was derived to extrapolate the height of the low-altitude satellites near the zenith using the angular velocity of the LEO satellite. This velocity was approximated through analysis of various exposures taken, at a fixed point of observation, over several nights.

Theory

Before observations can be done, it is important to establish the theory that will be essential in this research. The main goal of this project is to find a satellite's height at the zenith by using its angular velocity. To determine this, a mathematical expression is needed relating orbital height to what is captured during data collection. Using plate solving, the angular velocity can be determined from images displaying satellites. This means that the angular velocity of the satellite will need to be mathematically related to the height of the satellite at the time of observation, as seen from a position on Earth's surface. This mathematical relation has been derived using multiple known expressions, such as gravitational acceleration and centripetal acceleration. The full derivation is included in this theory section.

LEOs generally have low eccentricity orbits, which means these orbits are roughly circular (Riebeek, 2009). At every point in its orbit, the distance R from the satellite to the Earth's centre is approximately the same, as is the magnitude of the acceleration due to gravity. When considering uniform circular motion, the radial acceleration must be equal to the centripetal acceleration. Thus, the acceleration due to gravity of the satellite g_s can be written as:

$$g_s = \frac{{v_{tan}}^2}{R} \qquad (1)$$

In the expression above, R is the radius of the satellite's orbit and the velocity v_{tan} is the orbital velocity of the satellite. This speed is fixed, as different speeds would hinder circular orbital motion, since the satellite would either drift away from Earth or collide with it. The final equation will need to be expressed in terms of angular velocity. Orbital velocity can be replaced by the following relation between angular velocity ω_C (relative to the Earth's centre) and radius R of the satellite's orbit:

$$v_{tan} = \omega_C R \qquad (2)$$

This leads to the following expression of acceleration due to gravity:

$$g_s = \frac{{\omega_C}^2 R^2}{R} = {\omega_C}^2 R \qquad (3)$$

Additionally, acceleration due to gravity can be expressed using the relation between Newton's second law and the universal law of gravitation, which leads to the following expression for the satellite's acceleration due to gravity:

$$g_s = \frac{GM_E}{R^2} \qquad (4)$$

Combining both expressions yields:

$$\frac{GM_E}{R^2} = {\omega_C}^2 R \qquad (5)$$

$$GM_E = {\omega_C}^2 R^3 \qquad (6)$$

This formula describes the satellite's movement as seen from the centre of the Earth. However, the angular velocity measured is not from the viewpoint of Earth's centre, but from the observer's perspective, who is standing on the Earth's surface. The satellite's orbit appears to be elliptical from the camera's perspective, as the distance from the satellite to the observer is greater at the horizon than at the zenith. However, using short exposure times and observations exclusively near the zenith,

one could approximate the motion to be circular, since the distance from the satellite to the camera stays roughly the same.

The radius of the orbit around the Earth's centre R is the sum of Earth's radius R_E and the satellite's height h. Due to Earth's rotation along its own axis, its shape is compressed to a rotational ellipsoid with larger radii at equator level than at the poles. Therefore, a satellite moving in an orbit would have varying heights h depending on the location of observation. The measured angular velocity ω_O would refer to a theoretical circular orbit with a radius of h. With the tangential velocity of this orbit still being v_{tan}, the relationships $v_{tan} = \omega_O h$ and $v_{tan} = \omega_C(R_E + h)$ both hold true and can be combined:

$$\omega_C = \omega_O \frac{h}{(R_E+h)} \qquad (7)$$

This is illustrated below:

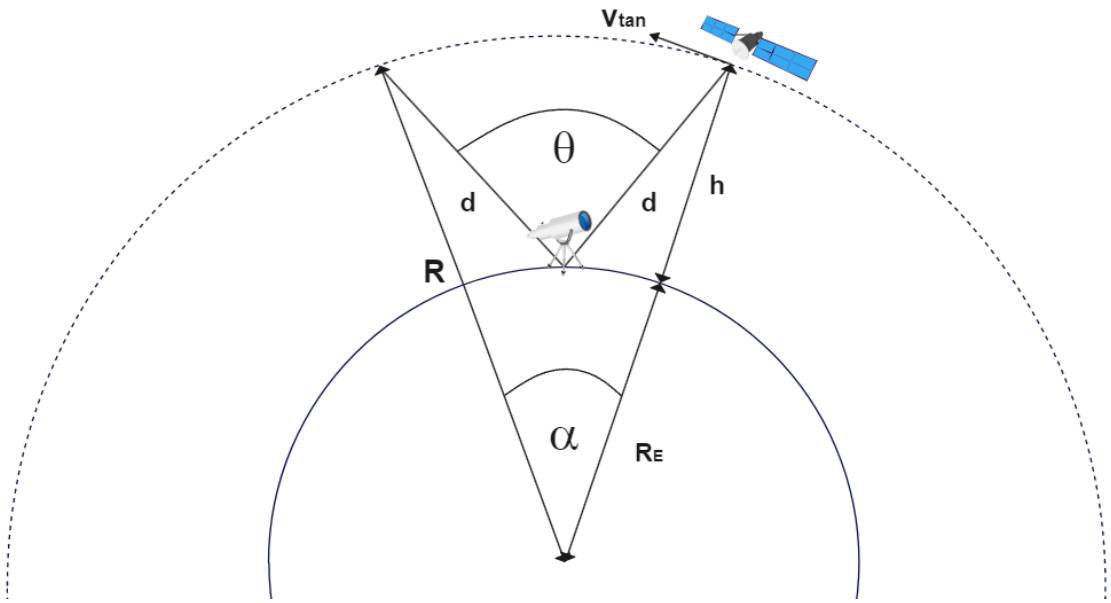

Figure 2.1: Diagram explaining relationships found in formula

This image underlines the importance of taking observations at the zenith. The closer the satellite moves towards the zenith, the more *d* approaches *h.* Similarly, at lower altitudes, the distance becomes larger. The relationship in (7) would therefore not apply anymore.

Equations (6) and (7) can now be combined and simplified to yield:

$$GM_E = (\omega_O \frac{h}{(R_E+h)})^2 (R_E + h)^3 \quad (8)$$

$$\frac{GM_E}{{\omega_O}^2} = h^2(R_E + h) \qquad (9)$$

In theory, an appropriate cubic equation, capable of determining the height of the satellite using the angular velocity relative to the observer, is established:

$$h^3 + h^2 R_E - \frac{GM_E}{{\omega_O}^2} = 0 \qquad (10)$$

In this equation, h is the height of the satellite relative to the observer, R_E is the radius of the Earth at the observer's location (found using the Earth ellipsoid model) and ω_O is the angular velocity of each satellite relative to the observer. G is the gravitational constant ($G \approx 6.674 * 10^{-11}\ Nm^2kg^{-2}$) and M_E is the mass of Earth ($M_E \approx 5.972 * 10^{24} kg$). Ultimately, the equation will provide 3 distinct solutions for the height, of which two will be negative and can be excluded. The positive value will be the experimentally determined height of the satellite.

A similar experiment performed in 2006 found the same formula (Earl, 2006). This provides an academic foundation for the accuracy of the equation derived above.

Materials and Methods

Materials

* DSLR camera (Canon Rebel T1i EOS 500D, 2009) (Canon, 2009)
* A laptop with APT software (HP 15s-eq2440nd, Ryzen i7, 64-bit, 2022)
* APT, Astro Photography Tool, software (version 4.20) (Incanus, 2023)
* Star tracker (Star Adventurer Pro pack, Sky-Watcher)
* Plate solving software (AstroImageJ) (Collins et al., 2011)
* Star angle calculator (Celestial Wonders) (Barret, n.d.)
* Heavens-Above database (Peat, n.d.)
* In-The-Sky.org (Ford, 2023)
* SkySafari Pro (Simulation Curriculum, 2021)
* Cubic equation solver (AKiTi, n.d.)

Methods

The equipment, consisting of the star tracker, the camera, and a laptop with APT, was set up after sunset and the star tracker was calibrated to Polaris. The camera was positioned level parallel to the ground with the lens facing the zenith and focused on the stars. Multiple plans with varying shutter time settings were programmed in the APT software on the laptop, which was connected to the camera. When a satellite was spotted and approached the camera's field of view, these plans were initiated, causing the camera to start taking exposures.

After the observations, the pictures with the clearest satellites, preferably close to the local zenith, were selected. These pictures were then plate-solved using AstroImageJ. Plate solving is a technique that delivers the celestial coordinates (right ascension and declination) of objects shown in the image. This is done by detecting known stars and assigning celestial coordinates to each pixel on an image.

Then, the arc length was calculated using the star angle calculator of Celestial Wonders and cross-checked using the arc length calculated by AstroImageJ. The angular velocity could be determined by dividing the arc length of the satellite track by the exposure time. The angular velocity, along with the local radius $R_{E,}$ was then plugged into the cubic function equation (10), together with the other known values, to find the height of the satellite from the observation point.

The satellites were then matched to those in the Heavens Above, In-The-Sky and SkySafari databases. This was done based on location data and the specific times the pictures were taken. With this information, the calculated heights could be compared with factual heights after which the error could be determined.

Observation conditions

On the night of June 15th, the first observation took place. There was little to no cloud cover until 1 am. Observations were made from 23:00 to 01:00. The starting outside temperature was 20 degrees Celsius and the final temperature was 15°C. During the night exposures of five and ten seconds were made with an ISO of 1200 or 1600.

On the night of June 16th, the second observation took place. There were clear skies throughout the night. Observations were made between 23:00 and 03:00. The outside temperature dropped throughout this time from 19 to 12°C. During the observation, the camera temperature dropped from 22 to 18°C. The observations had shutter times of five seconds and an ISO of 1600 or 1800.

On the night of June 24th, the third round of observations took place. There were little to no clouds. Observations were made from 23:00 until 03:15. During this time the outside temperature decreased from 22 to 15°C. The night's humidity was between 40% and 65%. The camera temperature varied between 25 and 19°C. The combination of these factors caused the lens to fog over often. Observations had a shutter time of five or eight seconds and an ISO of either 1500, 1600 or 1800.

On the night of the 25th of June, the fourth and last round of observations took place. There were several high clouds with the entire sky clouding over between 02:10 and 02:20. Observations were made between 23:00 and 03:00. The temperature dropped from 24 to 17°C with a humidity between 40% and 70%. The camera temperature fluctuated between 25 and 19°C. This caused the lens to fog over a bit. Observations were made with a shutter time of five seconds and an ISO of between 1400 and 2000.

These combined observation dates yielded a total of 1241 pictures in which approximately 108 satellites can be found at varying angles away from the zenith. Of these pictures, only 45 could be processed and are shown in this paper.

Results

Data

Date	Time	Satellite name	Image nr.	Ang. Disp. θ [°]	Ang. Disp. θ [rad]
16-Jun	00:22:00	Object U	1095	4.716	0.0823
17-Jun	00:30:00	STARLINK-2571	1300	3.625	0.0633
17-Jun	00:35:00	Cosmos 1674 Rocket	1309	3.123	0.0561
17-Jun	00:45:00	USA 234	1327	1.527	0.0266
17-Jun	00:56:21	STARLINK-5212	1368	3.135	0.0547
17-Jun	00:56:21	ALOS 2	1368	3.199	0.0558
17-Jun	01:15:15	STARLINK-5181	1467	3.482	0.0608
17-Jun	01:17:00	STARLINK-2121	1416	3.752	0.0655
17-Jun	01:20:00	STARLINK-2587	1424	5.226	0.0912
17-Jun	01:54:00	STARLINK-1396	1477	3.166	0.0553
17-Jun	01:59:29	STARLINK 5425	1487	5.141	0.0897
17-Jun	02:03:18	STARLINK-2008	1497	3.163	0.0552
17-Jun	02:38:24	STARLINK-2299	1225	3.856	0.0673
24-Jun	11:45:36	USA 238	1649	1.670	0.0291
25-Jun	00:21:06	2022-019U	1741	4.616	0.0806
25-Jun	00:33:01	USA 281	1757	1.908	0.0333
25-Jun	00:38:09	STARLINK-5417	1774	3.670	0.0646
25-Jun	00:45:42	STARLINK-3696	1788	5.818	0.1015
25-Jun	00:48:35	STARLINK-3681	1804	3.781	0.0660
25-Jun	00:48:35	Helios 1A Rocket	1804	3.721	0.0649
25-Jun	00:50:08	STARLINK-3691	1813	3.732	0.0651
25-Jun	00:50:19	STARLINK-3694	1814	3.740	0.0653
25-Jun	00:59:58	STARLINK-3669	1823	3.780	0.0660
25-Jun	01:02:04	STARLINK-3704	1832	3.721	0.0649
25-Jun	01:04:07	STARLINK-3690	1842	3.767	0.0657
25-Jun	01:33:36	Cosmos 1536 Rocket	1929	3.347	0.0584
25-Jun	02:24:25	Cosmos 2237	2011	2.357	0.0411
25-Jun	02:32:35	Cosmos 1892	2048	3.294	0.0575
25-Jun	02:39:26	GSLV R/B	2065	4.666	0.0814
25-Jun	11:30:29	STARLINK-1665	2114	3.837	0.0670
25-Jun	11:47:45	STARLINK-1451	2144	3.756	0.0656
25-Jun	11:48:05	Ariane 5 R/B	2146	3.426	0.0598
25-Jun	11:48:12	Cosmos 292	2147	2.994	0.0522
26-Jun	00:06:06	Cosmos 2322 Rocket	2165	2.196	0.0383
26-Jun	00:39:15	Emisat r	2189	4.705	0.0821
26-Jun	00:45:45	STARLINK-3694	2195	3.708	0.0647
26-Jun	00:46:20	Helios 1A	2199	3.822	0.0667
26-Jun	00:46:47	STARLINK-1419	2202	4.579	0.0799
26-Jun	00:55:09	STARLINK-1323	2234	3.590	0.0627
26-Jun	01:30:59	Cosmos 389 Rocket	2267	5.391	0.0941
26-Jun	01:31:24	SL-27 R/B	2270	5.015	0.0875
26-Jun	01:42:58	Cosmos 1356 Rocket	2282	3.424	0.0598
26-Jun	02:00:00	STARLINK-3787	2288	4.088	0.0713
26-Jun	02:30:04	WORLDVIEW-1	2308	4.207	0.0734
26-Jun	02:54:44	USA 234	2328	1.920	0.0335

Table A: Most probable angular displacements (derived as described below) and names of the satellites captured on the pictures. Angular displacements found after plate-solving.

Analysis

Observations were carried out as outlined in the method section, and plate-solved images yielded the angular displacement (θ) used in this analysis. The observed satellites' displacement was reflected as streaks in the images taken. Such streaks were often sufficiently distinct to denote a relatively clear position for the satellite at its first and last position captured in the image.

The AstroImageJ application's built-in tools for identifying ADU (Analog-to-Digital Unit) were utilized, assigning a brightness value to each pixel. Thus, five random samples of the light intensity along the satellite's main path were drawn and averaged, providing a standard average luminosity. This could be used to determine the most probable start and end positions of the satellite in the image. It was considered that the first and last sightings in an image would most likely be found at the ends. Under normal conditions, 80% of the average satellite light intensity was considered a sufficiently significant point to be considered the most probable, as the brightness along the whole satellite's path would not differ by more than 20% of the average luminosity. Past this point and along the line of displacement of the satellite, all points between the 80% and 20% average intensity mark were considered as possible positions in the angular displacement measurement. This possibly excluded positions outside this range which may have resulted in a larger error.

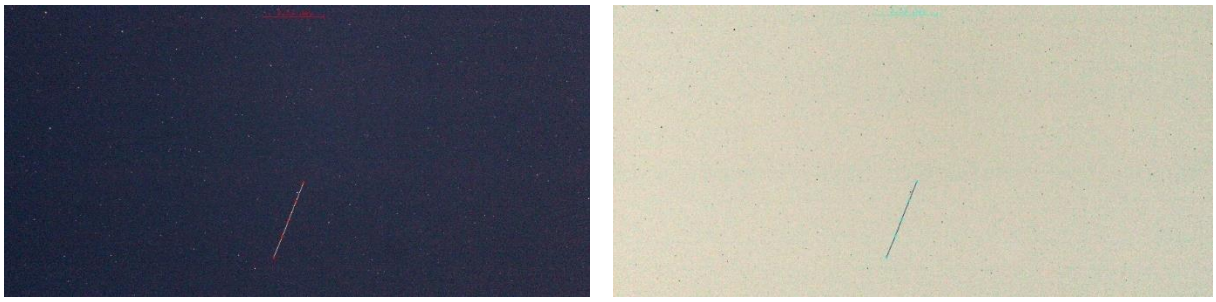

Figure 4.1: Five points on a satellite's trail, original image & inverted image

Skyglow captured in the image was accounted for in the calculations of these variations of satellite luminosity along its path:

$$I = 0.8(\overline{S} - \overline{Bg}) + \overline{Bg} \qquad (11)$$

$$i = 0.2(\overline{S} - \overline{Bg}) + \overline{Bg} \qquad (12)$$

In both equations, $\overline{S}$ is the average satellite luminosity and $\overline{Bg}$ is the average skyglow of the image. In equation (11), I is the intensity of the most probable first or last visible point of the satellite, with more than 80% of the average satellite's luminosity, this is a unitless value. In equation (12), i is the intensity of the furthest possible point it could have been captured at, at the 20% mark of the average intensity.

The angular displacement between points with intensity I and i at either side of the satellite streak was noted, and the sum of the two was considered the uncertainty $d\theta$.

Satellite height was computed as outlined in the theory section. Uncertainty concerning the height was obtained by first calculating the height with angular displacement θ, and then computing it again with (θ+$d\theta$). The difference between these two values represents the uncertainty. It is expected that the most probable height using θ will appear larger than the actual one. Nonetheless, the additional $d\theta$ uncertainty is supposed to account for this difference, it is therefore predicted that the actual height falls in between the two computed heights.

Additionally, to find a range where the formula could be used to establish a reasonable estimated height, the altitude *a* of the satellite with respect to the horizon was determined. This altitude can be described as the angular elevation of the celestial object towards the horizontal, as seen from the observer.

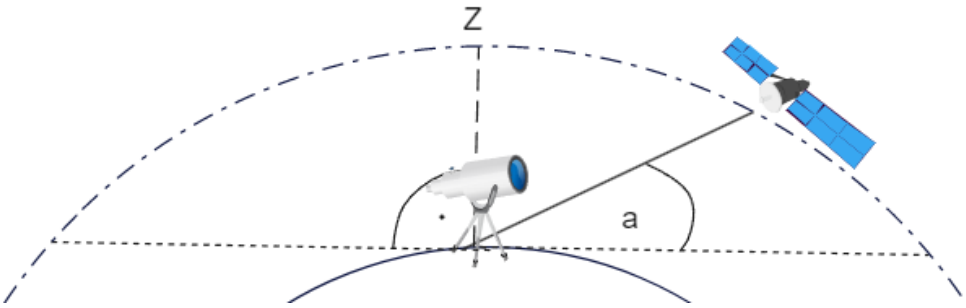

Figure 4.2: Satellite at an altitude a towards the horizontal. Z denotes the local zenith.

The local zenith is located at a 90° angle, appropriate altitudes should hence approach this value. Since the analysed picture already included the satellite's nearest point to the zenith, the most accurate altitude was obtained. A principal formula used in astronomy for star altitudes was fundamental, namely (Woolard, 2012):

$$\sin(a) = \sin(\phi_o)\sin(\delta) + \cos(\phi_o)\cos(\delta)\cos(h) \qquad (13)$$

Here, *a* is the altitude in degrees, where 90° would denote the zenith. Furthermore, ϕ_o and δ are the observer's latitude and the declination of the satellite, denoting its angle to the celestial equator. The declination and the right ascension were ascertained by applying the plate-solved images on AstroImageJ, whereafter the values were converted to degrees and hours respectively. The hour angle H describes how long ago the celestial object last transited through the observer's local meridian, in degrees. The following relationship allowed for the computation of H in degrees:

$$H = \frac{360}{24}(LST - \alpha) \qquad (14)$$

LST in equation (14) is the local sidereal time, and *α* is the right ascension of the satellite. While *LST* shows the angular distance of the local meridian towards the vernal equinox, *α* refers to the relation between the object's meridian and the equinox. The online Sidereal Time Calculator was utilized for the local sidereal time, which was then converted into the correct format (Borchia, 2023).

The exposure time of five seconds caused the satellite to be shown as a streak. The most reasonable *α* and *δ* in question were therefore those at its middle point. Utilizing these values and formulas (13) and (14), a reasonable estimate of the altitude is possible.

Analysis Satellite 2132

In this part, a satellite named 2132 was analysed to showcase the method used. The streak produced by this satellite was notable as it was at an angle of 89° from the horizon and it produced a boldly defined line. It was not possible to identify *Satellite 2132*. This satellite might have been a military reconnaissance satellite that was not registered in public domains.

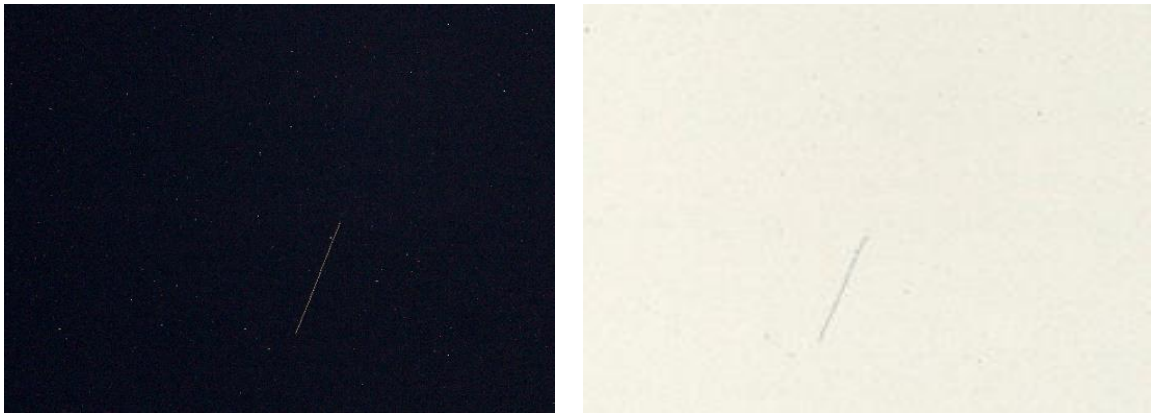

Figure 4.3: Satellite 2132 shown in original and inverted image

During the analysis of this satellite, endpoints and possible uncertainties in these endpoints were determined. This was done by evaluating the ADU at five points along the streak. The skyglow of the entire image was taken into account in equations (11) and (12) as $\overline{Bg}$, with the following values as a result:

Mean ADU ($\overline{Bg}$)	**ADU 1**	**ADU 2**	**ADU 3**	**ADU 4**	**ADU 5**	**Mean Sat. ADU ($\overline{S}$)**	**True 80% of ADU (I)**	**True 20% of ADU (I)**
22.262	97	100	103	114	107	104.2	87.812	38.650

Table B: ADU values for satellite 2132

The satellite was analysed and pixels with the 80% and 20% ADU values were chosen. The last points within the 80% ADU range established the boundaries for θ, as seen in figure 4.4 below:

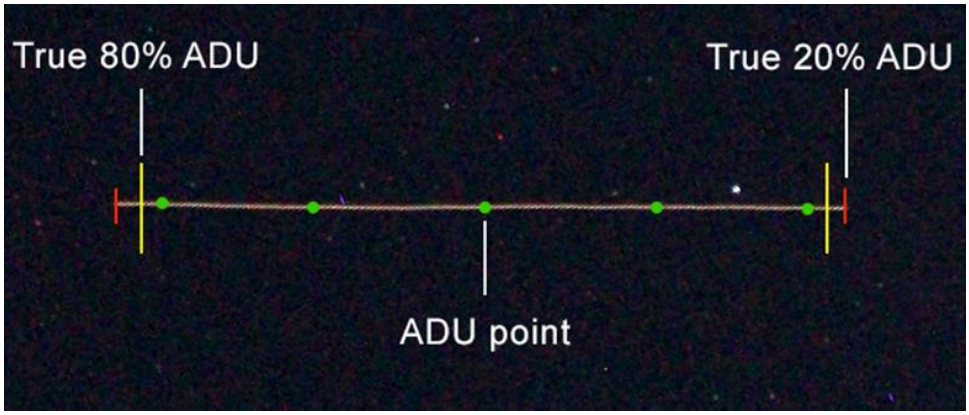

Figure 4.4: ADU points of satellite 2132

The image was then plate-solved as explained in the methods section. Figure 4.5 shows the plate solved image.

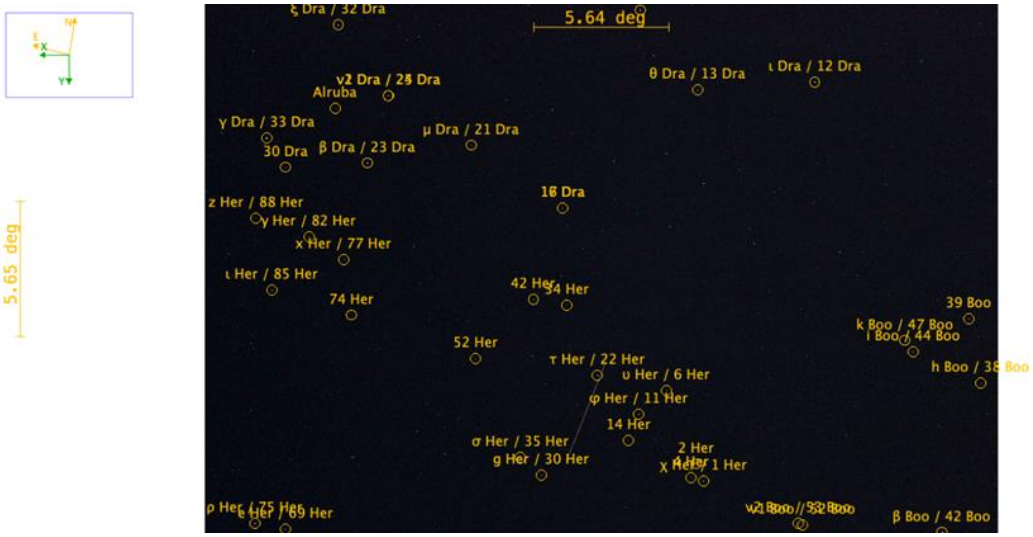

Figure 4.5: Plate solved image of satellite 2132

The right ascension and declination were determined for the endpoints shown in Figure 4.4. The angular distance between the 80% points was considered to be the most probable length of the streak. From this, the determined angular distance is found to be 4.4232°. This distance was calculated using the angular length tool. The uncertainty was defined to be the sum of the distances between the 80% and 20% points on either end. In this case, the uncertainty was 0.0333°.

The resulting angular distance (θ) was subsequently converted to radians, which resulted in a value of 0.0772 rad, and the angular velocity (ω_o) was computed as the quotient of the angular distance and the exposure time:

$$\omega_o = \frac{\theta}{t} = \frac{0.0772}{5} = 0.0154 \text{ rad/s}$$

Including the uncertainty $d\theta$, the maximum angular velocity can be found:

$$\omega'_o = \frac{\theta + d\theta}{t} = \frac{0.0772 + 0.00058}{5} = 0.0156 \text{ rad/s}$$

Once the value of ω_o had been determined the coefficients for the cubic equation (10) relating angular velocity to height were obtained. By solving the cubic equation, the positive root corresponded to the most probable height value *h*. This same process was then applied to the maximum angular velocity ω'_o, from which the minimum *h'* can be found. These values represent the height range.

Most probable height *h* [m]	**Minimum height *h'* [m]**	**dh [m]**
493723	491935	1787.9

Table C: Height values found for satellite 2132

When determining the specific satellite, the angular distance from the horizon (the altitude), the time of the photo and the direction of motion are taken into account. Using the celestial coordinates and our local coordinates, the altitude can be determined with equation (13). This altitude was found to be 89°. Nonetheless, no fitting satellite could be found, which makes comparison with an actual height value impossible.

Analysed Data

Satellite name	Image nr.	θ [°]	θ [rad]	θ+dθ [rad]	ω_o [rad/s]	ω'_o [rad/s]	h [m]	h' [m]	actual h [m]	% error	Altitude [°]
Cosmos 1356 R	***2282***	***3.779***	***0.0660***	***0.0664***	***0.0132***	***0.0132***	***574547***	***570517***	***569000***	***0.97***	***89.6***
STARLINK-3681	**1804**	**3.781**	**0.0660**	**0.0670**	**0.0132**	**0.0134**	**574235**	**566042**	**549400**	**4.52**	**87.6**
STARLINK-3704	1832	3.721	0.0649	0.0661	0.0130	0.0132	583122	573187	559400	**4.24**	**87.4**
STARLINK-1419	2202	4.579	0.0799	0.0804	0.0160	0.0161	477488	474644	460600	**3.67**	**86.5**
USA 238	1649	1.670	0.0291	0.0311	0.0058	0.0062	1241865	1170059	1272000	**-2.37**	**86.5**
STARLINK-1451	2144	3.756	0.0656	0.0664	0.0131	0.0133	577831	571800	547000	**5.64**	**86.3**
Cosmos 1536 R	1929	3.347	0.0584	0.0590	0.0117	0.0118	645397	639299	617000	**4.60**	**85.4**
Cosmos 1674 r	1309	3.213	0.0561	0.0564	0.0112	0.0113	671127	667813	621900	**7.92**	**85.3**
USA 281	*1757*	*1.908*	*0.0333*	*0.0391*	*0.0067*	*0.0078*	*1097304*	*943603*	*1079500*	***1.65***	***85.2***
STARLINK-3694	1814	3.740	0.0653	0.0659	0.0131	0.0132	580308	574776	558000	**4.00**	**85.1**
2022-019U	*1741*	*4.616*	*0.0806*	*0.0814*	*0.0161*	*0.0163*	*473830*	*469221*	*474000*	***-0.04***	***85.0***
STARLINK-3691	1813	3.732	0.0651	0.0660	0.0130	0.0132	581443	574280	559400	**3.94**	**84.8**
Helios 1A	2199	3.822	0.0667	0.0670	0.0133	0.0134	568275	565701	557000	**2.02**	**84.4**
STARLINK-1665	2114	3.837	0.0670	0.0675	0.0134	0.0135	566197	561864	547000	**3.51**	**84.4**
WORLDVIEW-1	2308	4.207	0.0734	0.0739	0.0147	0.0148	518197	515139	497500	**4.16**	**82.7**
STARLINK-3787	2288	4.088	0.0713	0.0722	0.0143	0.0144	532744	526899	506000	**5.29**	**82.4**
STARLINK-3694	2195	3.708	0.0647	0.0652	0.0129	0.0130	585114	580875	558000	**4.86**	**82.4**
Cosmos 2237	2011	2.357	0.0411	0.0426	0.0082	0.0085	900274	871585	851000	**5.79**	**82.3**
Object U	*1095*	*4.716*	*0.0823*	*0.0860*	*0.0165*	*0.0172*	*464112*	*444887*	*453000*	***2.45***	***82.1***
Emisat r	*2189*	*4.705*	*0.0821*	*0.0827*	*0.0164*	*0.0165*	*465142*	*462159*	*460040*	***1.11***	***82.0***
STARLINK-3669	1823	3.780	0.0660	0.0670	0.0132	0.0134	574367	566098	548000	**4.81**	**82.0**
Helios 1A R	1804	3.721	0.0649	0.0655	0.0130	0.0131	583122	578764	557000	**4.69**	**81.8**
Cosmos 389 R	*2267*	*5.391*	*0.0941*	*0.0945*	*0.0188*	*0.0189*	*408435*	*406002*	*399000*	***2.36***	***81.6***
SL-27 R/B	*2270*	*5.015*	*0.0875*	*0.0880*	*0.0175*	*0.0176*	*437237*	*434987*	*433000*	***0.98***	***81.2***
Ariane 5 R/B	*2146*	*3.426*	*0.0598*	*0.0603*	*0.0120*	*0.0121*	*631104*	*625964*	*636500*	***-0.85***	***81.2***
STARLINK-3696	1788	5.818	0.1015	0.1028	0.0203	0.0206	378550	364016	559400	**-32.33**	**81.0**
Cosmos 292	2147	2.994	0.0522	0.0526	0.0104	0.0105	717865	713149	681000	**5.41**	**80.8**
USA 234	2328	1.920	0.0335	0.0341	0.0067	0.0068	1091125	1074540	1102500	**-1.03**	**80.4**
STARLINK-2571	1300	3.625	0.0633	0.0659	0.0127	0.0132	598000	575142	553000	**8.13**	**79.9**
STARLINK-5417	1774	3.700	0.0646	0.0655	0.0129	0.0131	586328	578289	539500	**8.68**	**79.7**
Cosmos 2322 R	2165	2.196	0.0383	0.0387	0.0077	0.0077	962231	958136	845000	**13.87**	**79.4**
GSLV R/B	2065	4.666	0.0814	0.0818	0.0163	0.0164	468910	466849	448800	**4.48**	**79.0**
STARLINK-2299	*1225*	*3.856*	*0.0673*	*0.0694*	*0.0135*	*0.0139*	*563531*	*547380*	*553000*	***1.90***	***79.0***
Cosmos 1892	*2048*	*3.294*	*0.0575*	*0.0607*	*0.0115*	*0.0121*	*655357*	*622567*	*618000*	***6.04***	***78.7***
STARLINK-3690	1842	3.767	0.0657	0.0660	0.0131	0.0132	576256	574149	548000	**5.16**	**78.7**
STARLINK-1323	2234	3.590	0.0627	0.0633	0.0125	0.0127	603564	597501	553000	**9.14**	**78.3**
STARLINK-2121	1416	3.752	0.0655	0.0670	0.0131	0.0134	578482	565630	553000	**4.61**	**77.8**
ALOS 2	1368	3.199	0.0558	0.0563	0.0112	0.0113	673936	668155	637000	**5.80**	**74.3**
STARLINK 5425	1487	5.141	0.0897	0.0919	0.0179	0.0184	426905	417043	539500	**-20.87**	**70.8**
STARLINK-5181	1467	3.482	0.0608	0.0627	0.0122	0.0125	621420	603209	546000	**13.81**	**66.1**
USA 234	1327	1.527	0.0266	0.0283	0.0053	0.0057	1348902	1273967	1103000	**22.29**	**65.7**
STARLINK-2008	1497	3.163	0.0552	0.0576	0.0110	0.0115	681124	654256	547000	**24.52**	**65.2**
STARLINK-5212	1368	3.135	0.0547	0.0563	0.0109	0.01113	687097	668689	546000	**25.84**	**63.4**
STARLINK-1396	1477	3.166	0.0553	0.0570	0.0111	0.0114	680590	660183	553000	**23.07**	**61.8**
STARLINK-2587	1424	5.226	0.0912	0.0947	0.0182	0.0189	420177	405058	553000	**-24.02**	**59.5**

Table D: (from left to right) Satellite name, image number, angular displacement (degrees), angular displacement (radians), angular displacement (radians) + uncertainty, most probable angular velocity, maximum angular velocity, most probable height, minimum height, actual height, percentage height error, altitude.

Between the endpoints with intensity *I*, the most probable value for the angular displacement of the satellite was denoted by θ. Conversely, for the endpoints with intensity *i*, the maximum value was described by ($\theta + d\ \theta$). To find out the most probable height h and the minimal height *h'*, θ and ($\theta + d\ \theta$) respectively were inserted into the cubic equation. The percentage error related the computed height *h* with the satellite's actual one. Positive errors meant that *h* was higher than the actual value and vice versa.

Contrary to expectations, the actual heights of only a few of the satellites close to the zenith fell within the interval determined by the most probable and the minimum expected heights. This trend was also observed with satellites at altitudes of 87° *(1804, 1832).* The lowest altitude at which the satellites' height fell within the expected range was 79.0° *(1225)*. In most cases, the experimental height was higher than the actual value. Therefore, the percentage error was generally positive.

As the experimental values often failed to fall within the expected intervals, the percentage errors were considered to assess the validity of the cubic formula in equation (10).

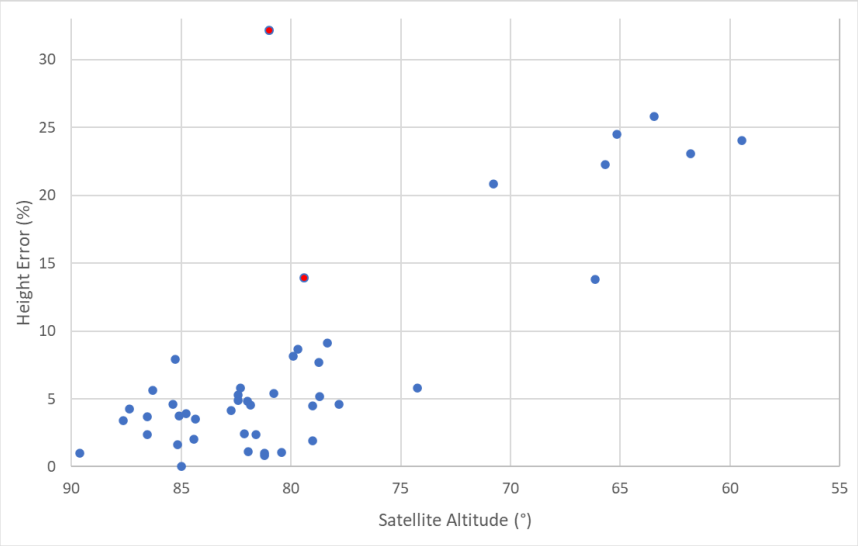

Graph 4.1: The absolute value of the height error from table A plotted against the satellite altitude at the time when the picture was taken. The red points correspond to satellites at an altitude included between 78° and 90° with an error bigger than 13%.

In Graph 4.1, the error appeared to increase when the altitude decreased. This could be explained by the fact that the approximation done in equation (7), which was used in establishing equation (10), ceases to hold true as the angle between the satellite and the zenith increases. All satellites that had altitudes lower than 70° lead to errors exceeding 10%. For those observed when even further from the zenith, the height error usually exceeded 20%, which suggested that the cubic formula found in (10) cannot be applied at low altitudes.

This trend was less noticeable within the 78°-90° interval. The errors had similar values throughout the interval (between 0.036% and 9.14%), with two exceptions at 80.99° and at 79.4°, where the errors exceeded 13%.

Finding the height percentage errors appeared to be a better tool to investigate the limits of the cubic equation than verifying if the heights fell within some expected intervals. Indeed, percentage errors seemed to fall within certain ranges for a given satellite altitude (e.g. the maximal error was 7.9% for satellites higher than 85°). However, the trends followed by the data were difficult to describe using the intervals formed by the most probable and minimum heights, because different situations appeared within the same altitude ranges (e.g. only some of the satellites higher than 80° fell within their error ranges).

Discussion

Data collection was suboptimal due to a variety of factors. The first of these is the limited number of possible observation days. The weather played a big role in this limitation. From the 18th until the 22nd of June, the cloud cover was too dense at night to observe any satellites. Due to technical difficulties, mainly concerning the cameras, observations on the 12th, 13th, 14th and 23rd were not possible, leaving only four observation dates.

However, even on the dates that observations were possible, technical difficulties prevented the capturing of all possible satellites. The camera had an issue focusing on the 16th, causing a significant time loss. On the 24th and 25th of June, the camera tended to fog over. On the 24th this meant having to clean and recalibrate the camera every 15 minutes, causing delays and missed satellites. This process had to be repeated less frequently on the 25th, but the SD card of the camera running out of space caused loss of observation time this day.

Generally, the camera was unable to record satellites passing by with magnitudes lower than 4.5. This meant that many satellites found to be passing near the zenith on Heavens Above, In-The-Sky and SkySafari could not be captured.

During the first two observation rounds, the 15th and 16th of June, the star tracker was used. This meant that the camera was turning to compensate for the rotation of the Earth. Consequently, the zenith was not at the centre of the camera frame at all times. This may have caused larger errors in data taken from those dates.

The error can also vary between images depending on the picture quality and camera focus. Due to temperature changes or human error, the camera changed focus during the observation nights, causing the images to be of varying quality. The different ISO settings throughout the nights might also have contributed to differences in the amount of light that can be captured and therefore the length of the trail. This led to several pictures being discarded during analysis, as the satellite ADU values were similar to the minimum background ADU, increasing uncertainty.

Having a standardised method to pinpoint the beginning and end of the trails within AstroImageJ was crucial. The 80-20 method used to determine the start and end of a satellite's trail made the measurements more consistent. If these values are chosen slightly differently, it can increase the uncertainty drastically. By using a standardised method to pick which pixels are the outer bounds, the uncertainty is decreased but not brought to zero. General glow and camera focus imperfections produced a "fade in/fade out" effect at either end of these streaks and the 80-20 method accounted for the introduced error in identifying these important positions of the satellite in the night sky.

Another error introduced during analysis might be a result of inconsistent ADU analysis. While it was attempted that the ADU values were taken at 5 largely equidistant points across each satellite streak, the first few pictures were not analysed this way, and 5 points were taken at random (usually all closer to one end of the satellite streak) by the analysis team. This led to skewed True 80% and 20% ADU values of the satellites, and one end had a better (smaller) 80:20 range than the other, increasing uncertainty on a few of the satellites.

Furthermore, the 80-20 method was challenged in the many occasions when stars, quasars and other bright objects in the sky appeared immediately after a satellite streak, increasing the calculated angular displacement, and affecting the experimental height.

It was determined after the analysis that the most accurate results were acquired when the celestial coordinates of the satellite ends were recorded from the outermost corner of pixels with the predetermined ADU values as compared to a measurement from the center of each pixel. This was unfortunately not done consistently during the analysis and could be an improvement when repeating this experiment.

The distance of the observer to the centre of the Earth was taken from the Earth ellipsoid model. The geoid model would have been more precise, since it most closely approximates the sea level on Earth, taking tides and wind out of the equation (NASA & DLR, 2004). The geoid distance was not used due to issues finding it for the specific observation location. The error caused by this omission would be rather negligible, considering that the largest possible difference between geoid and ellipsoid height worldwide is 106 meters (NASA & DLR, 2004). Still, it could have accounted for a small error.

Additionally, a large part of the error was introduced by the cubic polynomial relationship between height and angular velocity, shown by equation (10). This formula, as mentioned in the theory section, assumed the observed satellites' path to coincide with the zenith mid-observation. The formula appears to work for altitudes between 79° and 90°, while larger deviations cause it to break down. It was expected that the satellites would come close enough to the zenith to make the error insignificant. However, this still added a significant built-in error to every height computation, as most of them were at least a few degrees removed from the zenith. Furthermore, the use of this equation heavily restricted the sample of satellites usable for accurate analytic experimentation.

Theoretically, an alternate formula could be developed via vector analysis. This entails the consideration of the satellite's motion relative to the observer and relative to the centre of orbital motion which, although technically elliptical, is still near circular. This analysis could be enhanced further by considering the Coriolis effect on the motion of the satellites originated by the observer's and their frame-of-reference's rotation. Thus, the satellite's orbit could be more accurately depicted regardless of position and translation in the observer's night sky. Such evaluation, if done thoroughly, would enhance all facets of analysis and results, on top of allowing for a bigger, more diverse batch of satellites to be taken into account. However, for such depth to be achieved, extensive and highly technical physics theory and mathematical labour are required.

After the analysis, the satellites were compared to their counterparts found in the Heavens-above, In-the-Sky or SkySafari databases. This was not always possible due to these databases being incomplete. Some satellites did not appear in any of these databases, meaning comparison between calculated height and factual height was not possible. Additionally, some analysed streaks could have been assigned to the wrong satellites, leading to inaccuracies in their comparison.

Conclusion

The main goal of this research was to determine whether it is possible to calculate the height of satellites near the zenith using their angular velocity. The results show that the majority of the computed heights were within 8 % from the actual height, when limited to altitudes between 79° and 90°. Within these constraints, it is possible to determine an accurate height of a satellite by its angular velocity.

Various factors can explain the size of the errors found in this research. Some of these factors are the presumptions made in the formula, the difficulty determining the start and end point of the trails, and the use of the ellipsoid model. Moreover, the data collection itself was limited by weather, technical difficulties and low magnitude satellites.

Any further research might benefit from the use of an alternative formula instead of the formula derived in this research. This could yield a lower margin of error and might allow for satellites at more diverse altitudes to be included.

References

AKiTi. (n.d.). *Cubic Equation Solver.*
http://www.akiti.ca/Quad3Deg.html

Barret, F. (n.d.). *Calculate Angular Distance Between Two Stars*. Celestial Wonders.
http://celestialwonders.com/tools/starAngleCalc.html

Borchia, D. (2023, June 5). *Sidereal Time Calculator.* Omni Calculator.
https://www.omnicalculator.com/everyday-life/sidereal-time

Canon. (2009). *Canon EOS Rebel T1i EOS 500D instruction manual*.

Earl, M.A. (2006). Determining the Orbit Height of a Low-Earth-Orbiting Artificial Satellite Observed near the Local Zenith. *The Journal of the Royal Astronomical Society of Canada, 100*(5), 199-203.
https://rasc.ca/sites/default/files/publications/JRASC-2006-10-hr.pdf

Ford, D. (2023). *Live World Map of Satellite Positions.* In-The-Sky.org.
https://in-the-sky.org/satmap_radar.php

Fraknoi, A., Morrison, D., Wolff S. (2022). *Astronomy 2e.* Openstax.
https://openstax.org/books/astronomy-2e/pages/19-2-surveying-the-stars

NASA, DLR. (2004). *Earth's Gravity Definition.* Gravity Recovery and Climate Experiment.
https://www2.csr.utexas.edu/grace/gravity/gravity_definition.html

Peat, C. (n.d.). *Daily predictions for brighter satellites.* Heavens Above.
https://www.heavens-above.com/AllSats

Riebeek, H. (2009, September 4). *Catalog of Earth Satellite Orbits*. NASA Earth Observatory.
https://Earthobservatory.nasa.gov/features/OrbitsCatalog

Stewart, K. (n.d.). low Earth orbit. Encyclopedia Britannica.
https://www.britannica.com/technology/low-Earth-orbit

Tatem, A.J., Goetz, S.J., Hay, S.I. (2008). Fifty Years of Earth-observation Satellites. *American Scientist. 96* (5): 390–398. doi:10.1511/2008.74.390

Woolard, E. (2012). *Spherical Astronomy*. Elsevier.

Software

Collins, K., Eastridge, K., Kielkopf, J. (2011). *AstroImageJ* (Version 5.2.0.16) [Computer Software].
https://www.astro.louisville.edu/software/astroimagej/

Incanus Ltd. (2023). *Astro Photography Tool* (Version 4.20 PlateSolve 3) [Computer Software].
https://astrophotography.app/

Simulation Curriculum. (2021). *SkySafari 7 Pro* (version 7.2.0) [Mobile App].
https://skysafariastronomy.com/

Appendix A

Task division

Tasks writing paper

Introduction	Miguel
Theory	Laura, Nils
Materials and Method	Emma
Results	Mathias, Nils, Kateryna
Discussion	Smrithi, Indra, Samir, Emma, Miguel
Conclusion	Collective effort
Cohesion work + references	Laura, Emma

Tasks outside of writing

Observation	Emma, Laura, Mathias, Nils
Mathematical Analysis	Nils, Mathias
Identifying satellites	Kateryna, Laura
Plate Solving + Analysis	Smrithi, Kateryna, Samir
Poster Design	Indra

Appendix B

Complete data analysis and images used in this research can be found on the google drive file 'Satellite Project Drive' accessed through the following link:
https://drive.google.com/drive/folders/1nEZELdB6_W8Qf7Y8kF0ULLtJyz5hQ7ZL?usp=sharing